

Magnetic anisotropy and dipolar interactions in the frustrated triangular-lattice magnet NaGdS₂

J. Grumbach^{1,*}, E. Häußler², S. Luther³, J. Sichelschmidt⁴, K. M. Ranjith⁴, T. Herrmannsdörfer³, M. Rotter⁵, S. Granovsky¹, H. Kühne³, M. Uhlarz³, J. Wosnitza^{1,3}, H.-H. Klauß¹, M. Baenitz⁴, T. Doert², and M. Doerr¹

¹*Institut für Festkörper- und Materialphysik, Technische Universität Dresden, 01062 Dresden, Germany*

²*Fakultät für Chemie und Lebensmittelchemie, Technische Universität Dresden, 01062 Dresden, Germany*

³*Hochfeld-Magnetlabor Dresden (HLD-EMFL) and Würzburg-Dresden Cluster of Excellence ct.qmat,*

Helmholtz-Zentrum Dresden-Rossendorf, 01328 Dresden, Germany

⁴*Max-Planck-Institut für Chemische Physik fester Stoffe, 01187 Dresden, Germany*

⁵*McPhase Project, 01159 Dresden, Germany*



(Received 31 January 2025; revised 25 March 2025; accepted 26 March 2025; published 4 April 2025)

In this comprehensive study, we present results of bulk measurements (magnetization, specific heat, ac susceptibility, thermal expansion, and magnetostriction) combined with local methods such as nuclear magnetic resonance (²³Na NMR) and electron spin resonance (ESR) and simulations (*McPhase*) on polycrystalline and single-crystalline NaGdS₂ samples. The rare-earth delafossite NaGdS₂ is a triangular-lattice magnet with $S = 7/2$ spin-only Gd³⁺ moments with suppressed single-ion anisotropy. In our study, we estimate that NaGdS₂ has a weak antiferromagnetic exchange ($J_H/k_B \approx 52$ mK) and signs of long-range magnetic order are absent down to lowest temperature. However, indications of short range magnetic order are found below 180 mK in the ac susceptibility and thermal expansion. Our results indicate an interplay of Heisenberg-type and dipolar exchange. Due to the large moment of the Gd³⁺ ions, one expects a strong impact of the dipolar coupling in NaGdS₂, in contrast to the related NaYbS₂. ESR and ²³Na NMR measurements, indeed, indicate the formation of short-range ferromagnetic correlations. NaGdS₂ appears to be a rare system, in which magnetic order is suppressed by a competition between Heisenberg and dipolar interactions.

DOI: [10.1103/PhysRevB.111.144404](https://doi.org/10.1103/PhysRevB.111.144404)

I. INTRODUCTION

Selected, mostly planar, lattices with a defined spin arrangement (honeycomb, triangle, square) are suitable to realize a spin-liquid (SL) state. In addition to the crystal structure, the type of exchange interaction plays a decisive role. In recent years, some 4*f*-based quantum magnets have emerged as excellent candidates for the research of spin-liquids and other unusual magnetic states, as some Kramers ions host a quasi spin-1/2 state at low temperatures.

Promising candidates for quantum spin-liquid materials based on triangular lattices are rare-earth delafossite compounds (α -NaFeO₂ structure type) of composition ARX_2 . Thereby *A* denotes a monovalent ion (mostly an alkali metal), *R* denotes a trivalent rare-earth ion, and *X* stands for a chalcogenide. Delafossites crystallize in the centrosymmetric trigonal $R\bar{3}m$ space group. The structure is built out of a two-dimensional (2D) network of AX_6 and RX_6 octahedra [see Fig. 1(b)] [1,2]. Ideal triangular rare-earth planes are separated by nonmagnetic layers [see Fig. 1(a)], providing delafossites as triangular-lattice quantum magnets.

Most prominent members of the compound family are NaYbX₂, where the spin-liquid ground state seems to be well achieved [3]. In other cases, several types of antiferromagnetically ordered compounds were found. The list of

compounds is constantly growing. For instance, NaYbO₂ [4] NaYbS₂ [5,6], NaYbSe₂ [7,8], KYbS₂ [9], CsCeS₂, CsYbSe₂ [10], and KHoSe₂ [11] display possible quantum spin liquid ground states, whereas KCeS₂ [12,13] and KCeSe₂ [14] show long-range magnetic order. In addition, the non-Kramers-ion material KTmSe₂ [15] was also investigated, also revealing absent long range order.

Here, we report on the rare-earth delafossite NaGdS₂. This compound is a triangular-lattice magnet with 4*f*⁷ $S = 7/2$ spin-only Gd³⁺ moments without single-ion anisotropy. Indeed, in Gd compounds often weaker influences such as dipolar contributions or effects due to the crystal symmetry affect anisotropies. So far, no magnetic order has been reported for NaGdS₂, which means that it is a possible spin liquid. This also favors the system as a superior cooling material for adiabatic demagnetization applications [16]. However, due to the large spin moment and less spin-orbit entanglement, one would actually expect order. In contrast, other possible Gd-based spin liquids have a more three-dimensional exchange network [17,18]. In the 4*f*-ion relative NaYbS₂ the absence of magnetic order and the spin-liquid ground state originate from bond-dependent frustration due to spin-orbit entanglement [3].

In this context, the question arises, which interactions compete with each other in NaGdS₂ and what additional influence the geometric frustration of the triangular lattice has. For temperatures above 1 K, the magnetic exchange (Heisenberg) is the decisive interaction, whereas in the mK temperature range

*Contact author: Justus.Grumbach@tu-dresden.de

the dipolar interaction can also become important. The latter is often much weaker than the magnetic exchange and is only used as a correction variable that extends the range of the coupling strength of the nearest-neighbor interactions J_1 and J_2 , which leads to spin liquid behavior [19]. Of particular interest are, therefore, compounds in which the dipole exchange is in the similar energy range as the exchange coupling. Especially for Gd^{3+} compounds with large spin moment stronger dipolar effects are expected compared to Yb^{3+} compounds, since the interactions are quadratic with the magnetic moment. Theoretical work on compounds with triangular lattice also points to the importance of dipolar ordering especially for Gd^{3+} compounds [19,20]. Also experimental work on triangular lattices with Gd^{3+} discusses the role of dipolar interactions. One example is $\text{KBaGd}(\text{BO}_3)_2$, where magnetic order was detected at $T_N = 262$ mK [21,22]. This compound family seems to be a good example for very weak exchange interaction; even a related Yb^{3+} compound orders via dipolar interactions [23]. Our compound NaGdS_2 has the advantage that randomness of the ion distribution can be neglected, so that the presence of distributed exchange couplings should be far less significant.

II. EXPERIMENTAL

A. Synthesis

We grew NaGdS_2 powder samples and crystals at 1050°C from a Na_2CO_3 or Na_2S flux, respectively, in a protective argon atmosphere by a slightly modified procedure as reported by Masuda *et al.* [24].

For the powder samples, we mixed dried Na_2CO_3 (4239.6 mg, 40 mmol, 40 equivalents) with 1 equivalents of Gd_2O_3 (Alfa Aesar, 99.999 %) in a porcelain mortar and filled in a glassy carbon boat, which was placed in a ceramic tube inside a tubular furnace. After flushing all pipes and a 1 l flask containing liquid CS_2 with argon for 30 minutes, we heated the furnace up to 1050°C within three hours (≈ 5.7 K/min) under a stream of argon of approx. 21/h. While dwelling for 30 minutes, CS_2 was transported to the reaction zone by bubbling argon (≈ 51 /h) through the reservoir. Under an unloaded stream of argon, we cooled the furnace to 600°C within three hours (2.5 K/min) and without further control to room temperature. After dissolving the solidified flux with distilled water, we filtered off the target compound and washed it with ethanol. Leftovers of small black particles, presumably carbon, were decanted after ultrasonic treatment in ethanol. The remaining product was found to consist of mostly intergrown agglomerates of small colorless hexagonal crystals (1–10 μm).

For growing larger crystals up to 800 μm in diameter, we used dried Na_2S as flux with the same molar ratio in the mixture. During the synthesis, the dwelling time was prolonged to one hour, and the cooling rate was decreased to 1.25 K/min. One of the resulting crystals is shown in the inset of Fig. 2. We evaluated the phase purity of the samples by x-ray powder diffraction measured on a Stoe Stadi P diffractometer using $\text{Cu-K}\alpha_1$ radiation, also shown in Fig. 2.

B. Measurement methods

We performed magnetization measurements on the powder samples using a SQUID magnetometer down to 0.5 K providing a general magnetic characterization. For our mea-

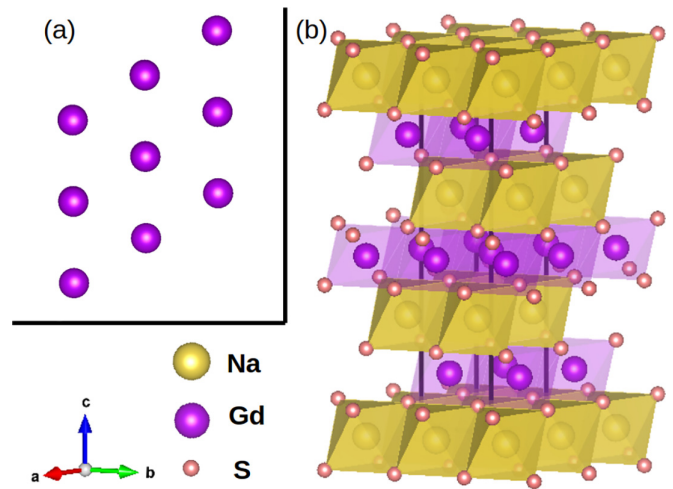


FIG. 1. Crystal structure of NaGdS_2 with (a) hexagonal layers of Gd^{3+} ions viewed along [001] and (b) alternating stacking of nonmagnetic and magnetic planes of NaS_6 and GdS_6 octahedra. The visualization was done in VESTA [25].

surements on single crystals, we used a VSM system in a cryo-free system (CFMS), which operates as a liquid-helium closed-cycle system, between 1.5 and 300 K and magnetic fields up to 12 T. We applied sweep rates of 0.1 T/min to 0.3 T/min and 0.1 K/min to 1 K/min to assure full thermalization of the samples. The plate-like single crystals were mounted with the basal plane on two different non-magnetic holders in order to do measurements in-plane and out-of-plane.

We measured the magnetic susceptibility down to 60 mK using an ac-method by employing a compensated pick-up coil system installed in a $^3\text{He}/^4\text{He}$ dilution refrigerator, capable of reaching fields up to 16 T. The sweep rate of the temperature was between 1 and 1.5 mK/min.

For temperature- and field-dependent dilatometry measurements, we used a capacitive tilted-annulus dilatometer cell

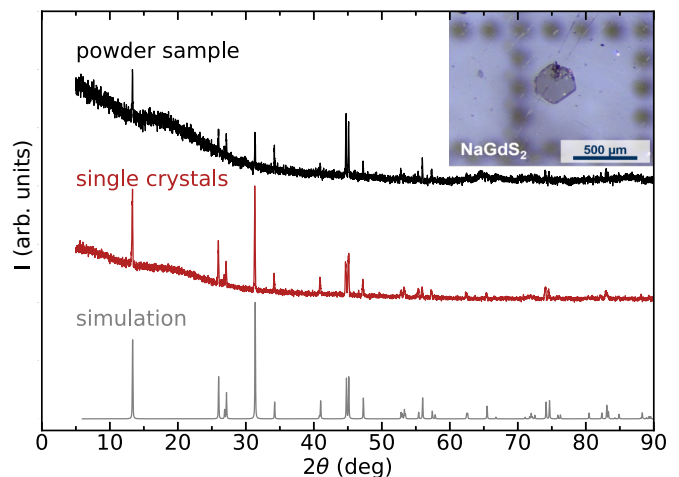


FIG. 2. Powder diffraction patterns of the two NaGdS_2 batches used in this study. Selected single crystals were ground to powder to measure the spectrum. One of the transparent single crystals is shown in the inset.

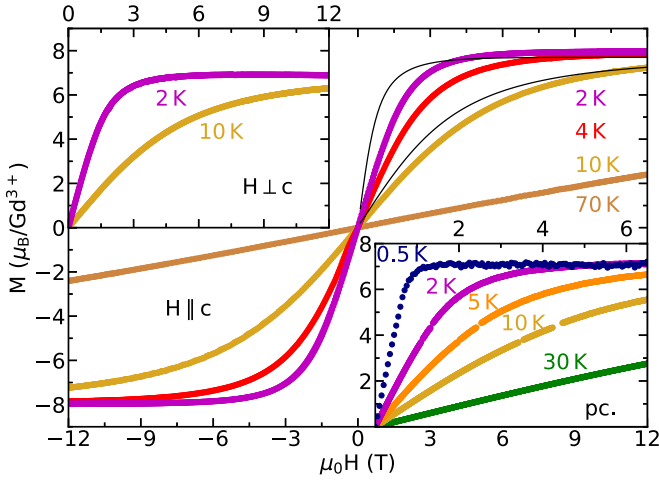


FIG. 3. Field-dependent magnetization of single-crystalline NaGdS₂ for $H \parallel c$ (main figure) and $H \perp c$ (left inset) as well as polycrystalline NaGdS₂ (right inset) at various temperatures. The solid lines show Brillouin functions.

with a sensitivity to relative length changes of $\sim 10^{-7}$ [26] in a dilution refrigerator.

We measured the specific heat in the mentioned CFMS using an ac method. A single crystal of a mass of 40 μg was glued to a $100 \times 100 \mu\text{m}^2$ membrane, which is equipped with a heater. For measuring the temperature, we used a semiconducting Cernox resistor.

Further, we investigated the electron spin resonance (ESR) of a NaGdS₂ single crystal. We probed the ESR by detecting the power P absorbed by a transversally applied magnetic microwave field. For improved signal-to-noise ratio, we recorded the first derivative of the absorbed microwave power, dP/dH . We used a continuous-wave ESR spectrometer at the X-band (9.4 GHz) and employed a He-flow cryostat to reach temperatures down to 4 K. The measured resonance spectra were described with a Lorentzian shape including the influence of the counter-rotating component (“counter res-

onance”) of the linearly polarized microwave field [27,28]. From this fit, we obtained the linewidth ΔH and resonance field H_{res} .

We used a conventional pulsed NMR method on the ^{23}Na nuclei (nuclear spin $I = 3/2$) in the temperature range between 2 and 295 K, at a fixed frequency of 35 MHz. We mixed NaGdS₂ powder with paraffin, heated it up, shook it, and then cured it to randomize the grains. The field-sweep spectra are obtained by integration over the spin echo in the time domain. The powder spectra are modeled with an anisotropic shift tensor. We determined tensor components in the ab plane and along the c direction.

III. RESULTS

A. Magnetization

The magnetization of the polycrystalline sample [see right inset of Figs. 3 and 4(a)] shows the absence of magnetic order down to 0.5 K, a saturation moment of $7.2 \mu_{\text{B}}$ at a saturation field of 1 T at 0.5 K (in contrast to about 15 T for NaYbS₂ [5]) and a rather small negative Curie-Weiss temperature of -1.9 K [see Curie-Weiss fit to the dc-susceptibility data in the right inset of Fig. 4(a)]. The negative Curie-Weiss temperature indicates an overall dominant antiferromagnetic exchange between the moments, consistent with predictions [29]. We further investigated the magnetic anisotropy by measuring the magnetizations for fields aligned in plane ($H \perp c$) and out of plane ($H \parallel c$), shown in Fig. 3. The saturation magnetization for $H \parallel c$ ($7.96 \mu_{\text{B}}$) is slightly larger, than for $H \perp c$ ($6.90 \mu_{\text{B}}$). From Curie-Weiss fits to the dc-susceptibility data, we determined very similar, but larger Curie-Weiss moments of $\mu_{\text{eff}}^{\parallel} = 8.6 \mu_{\text{B}}$ and $\mu_{\text{eff}}^{\perp} = 8.8 \mu_{\text{B}}$. This, in company with the saturation magnetizations may be caused by modified g -factors in the actual crystal, which motivated our ESR measurements. For reference, the effective Curie-Weiss moment for the free Gd³⁺ ion is given by $\mu_{\text{eff}} = g\sqrt{J(J+1)} \mu_{\text{B}} = 7.94 \mu_{\text{B}}$ (assuming $g \approx 2$), whereas the saturation moment in the magnetization is $M_{\text{sat}} = gJ\mu_{\text{B}} = 7.01 \mu_{\text{B}}$.

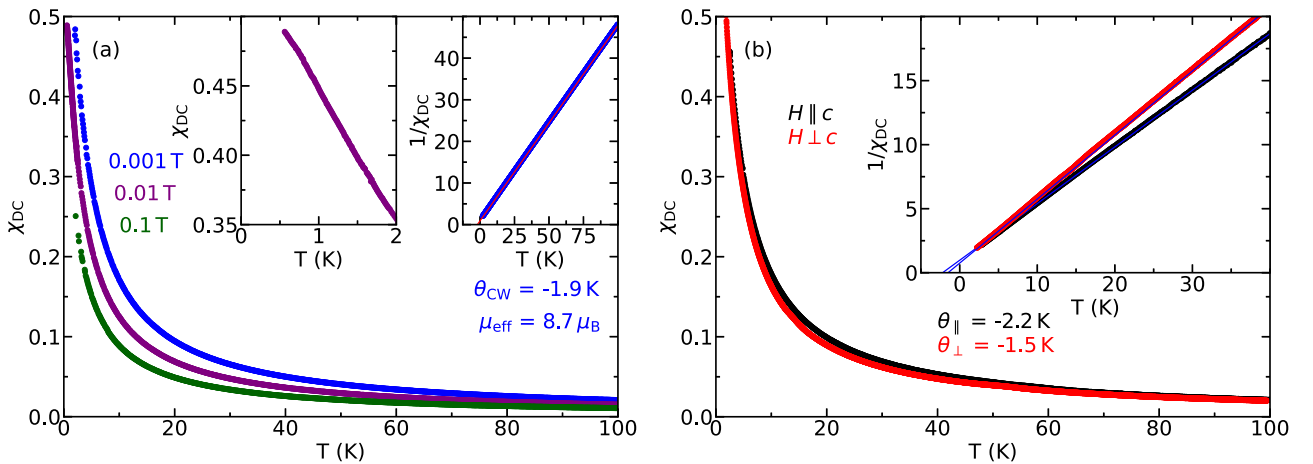


FIG. 4. Temperature dependence of the magnetic dc susceptibility of (a) polycrystalline material and (b) single crystals of NaGdS₂. The left inset in (a) shows an enlargement of the data in $\mu_0 H = 0.01$ T below 2 K revealing the absence of magnetic order down to 0.5 K. The right inset in (a) and the inset in (b) show the inverse susceptibility and Curie-Weiss fits (solid lines) indicating paramagnetism and revealing a small anisotropy in the single crystal (b).

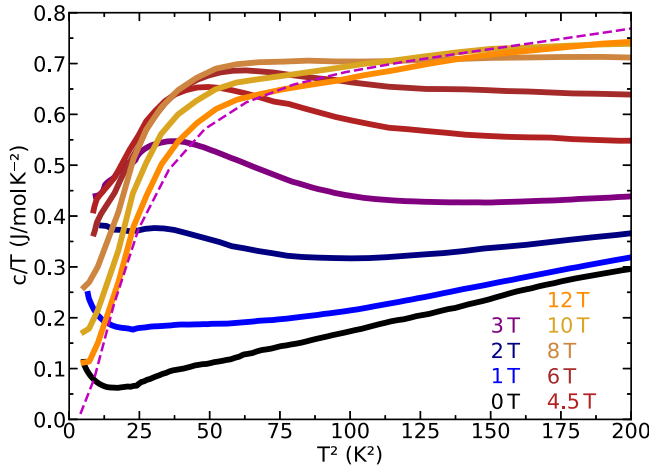


FIG. 5. Specific heat divided by T vs. T^2 at different magnetic fields. In zero and low magnetic fields the upturn at lowest temperatures indicates magnetic contributions. At higher fields a broad Schottky-like anomaly develops. The dashed line shows the specific heat calculated for a 8-level Schottky anomaly at 12 T.

Interestingly, also the Curie-Weiss temperatures differ slightly for the two directions ($\theta_{\parallel} = -2.2$ K and $\theta_{\perp} = -1.5$ K) [see Fig. 4(b)]. A small anisotropy exceeds the respective error bars of ± 0.2 K. Assuming only Heisenberg interactions, this indicates a larger coupling of the moments along the c direction than in the ab plane. This is in contrast to NaYbS_2 , for which a strong anisotropy exists with $\theta_{\parallel} = -4.5$ K and $\theta_{\perp} = -13.5$ K [5]. This points towards a different origin of the anisotropy. While for NaYbS_2 crystal-field effects dominate, for NaGdS_2 dipolar interactions are of major importance. The stronger dipolar interaction in the plane, due to shorter interatomic distances, might be the reason for the stronger reduction of the Curie-Weiss temperature when the magnetic field is oriented in-plane.

We further made a comparison of our magnetization data to paramagnetic Brillouin functions for $H \parallel c$ (Fig. 3). For that we used the g -factor obtained by ESR, as discussed later. The differences are only small, with delayed polarizations (similar as reported in [21]), which hint at the presence of only weak antiferromagnetic exchange contributions. Hence, down to 2 K, we can describe NaGdS_2 as a paramagnet with weak exchange and small anisotropy.

B. Specific heat

We measured the specific heat as function of temperature at various magnetic fields up to 12 T. The data at zero field follow a classical Debye-like behavior and reach the Dulong-Petit value at about 200 K (data not shown). No sharp feature hinting at a phase transition is present above 2 K. In zero field, we observe an upturn in c/T below 4 K (Fig. 5). This indicates an onset of magnetic correlations. In applied magnetic fields, this onset is gradually disappearing and a broad magnetic contribution appears at 1 T and higher fields, shifting to higher temperatures with increasing fields. This anomaly can be explained assuming 8-level Schottky anomalies of the Gd^{3+} $S = 7/2$ ground state.

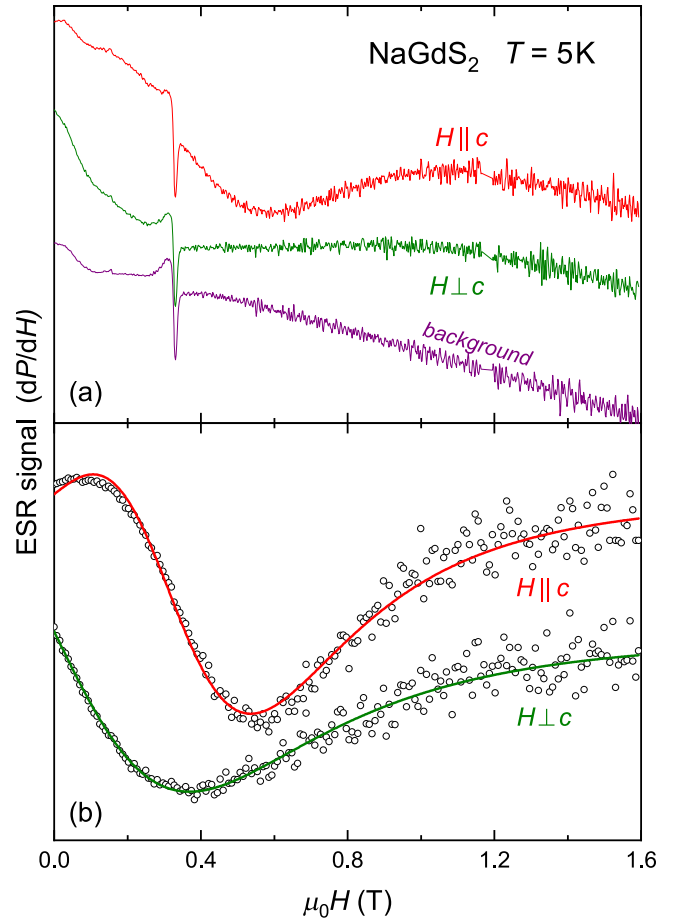


FIG. 6. Typical ESR spectra of NaGdS_2 at 5 K. (a) Raw ESR spectra for in-plane ($H \perp c$) and out-of-plane ($H \parallel c$) external field directions including a prominent background. (b) ESR spectra after subtracting the background. Solid lines denote Lorentzian line shapes which also take the counter resonance into account.

For multilevel systems, an equation of the energy of n degenerate levels can be derived to be

$$E = N \frac{\sum_{r=0}^{n-1} E_r \exp\left(-\frac{E_r}{k_B T}\right)}{\sum_{r=0}^{n-1} \exp\left(-\frac{E_r}{k_B T}\right)}, \quad (1)$$

from which the contribution to the specific heat results by differentiation with respect to the temperature.

In our case we assumed equidistant energies, Zeeman-split by the external magnetic field. We neglected inner magnetic fields, assuming this effect to be low as deduced before. The resulting Schottky-curve shown for the data at 12 T (Fig. 5) as an example. Despite the simplicity of the model, the peak is resembled reasonably well, showing that the Schottky-anomaly due to Zeeman-splitting is the main contribution of this peak.

C. Electron spin resonance

We investigated the ESR of a small ($m \simeq 0.02$ mg) NaGdS_2 single crystal. As shown in Fig. 6(a) the obtained spectra are weak as compared to the background, and broad

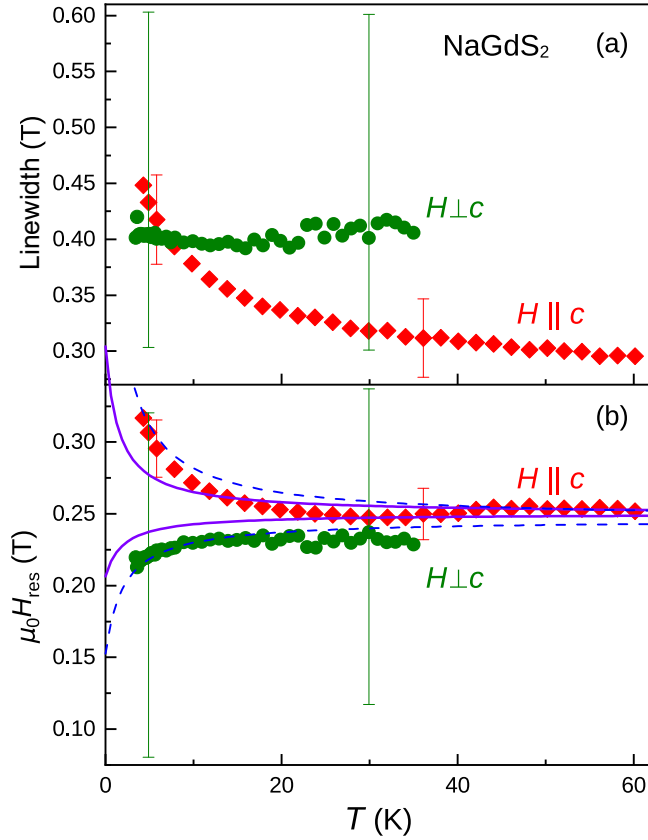


FIG. 7. Temperature dependence of (a) the ESR linewidth and (b) resonance field for $H \parallel c$ and $H \perp c$. At 60 K, the resonance field corresponds to an effective g -factor $g_{\parallel} = 2.6(7)$. Solid lines denote a molecular-field description of $\mu_0 H_{\text{res}}$, using Eqs. (2) and (3) with θ_{\perp} and θ_{\parallel} as determined by χ_{DC} [see Fig. 4(b)]. Dashed lines are results from the same equations based on simulated Curie-Weiss temperatures (see discussion).

in field. We found such spectra for temperatures up to about 60 K, above which the sample signal reaches the detection limit. Prior fitting with a symmetric Lorentzian line shape (solid lines), we subtracted the background yielding the spectra as displayed in Fig. 6(b). This finding for the shape is in contrast to the non-Lorentzian shape reported in a previous ESR study of Gd^{3+} spins on a triangular lattice for TiGdSe_2 [30]. We determined the ESR g values via the resonance field H_{res} which appears to be strongly anisotropic. This points to internal fields adding to the external field most effectively in the plane.

Figure 7(a) shows the temperature dependence of the ESR linewidth ΔH , while Fig. 7(b) shows that of the resonance field H_{res} for $H \parallel c$ and $H \perp c$. The small signal amplitude relative to the background signal causes large error bars for $H \perp c$, see Fig. 6(a).

Towards low temperatures, the growing influence of spin correlations lead to an increase of ΔH as well as to increasing internal fields, which affect the resonance field H_{res} . The latter qualitatively resembles the behavior of the Yb^{3+} ESR in NaYbS_2 [31], for which a molecular-field model [32] of the anisotropic Yb–Yb interaction provided a reasonable descrip-

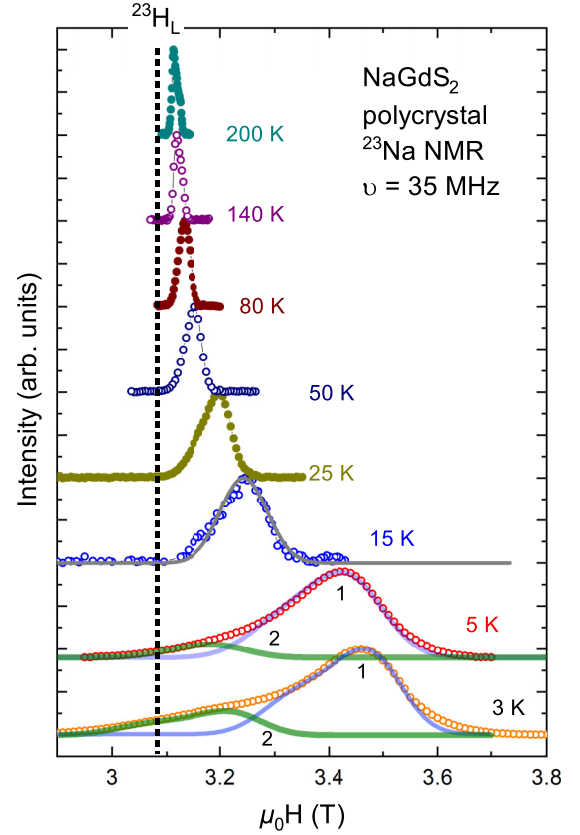


FIG. 8. ^{23}Na field-sweep NMR spectra taken at 35 MHz. The solid lines represent simulations (see text). The vertical dotted line indicates the Larmor field for ^{23}Na .

tion. Adapting this molecular-field model to the temperature dependence of the resonance field results in

$$H_{\perp \text{res}}(T) = H_{\perp \text{res}}^0 \left(1 + \frac{\theta_{\perp} - \theta_{\parallel}}{T - \theta_{\perp}} \right)^{-\frac{1}{2}}, \quad (2)$$

$$H_{\parallel \text{res}}(T) = H_{\parallel \text{res}}^0 \left(1 - \frac{\theta_{\perp} - \theta_{\parallel}}{T - \theta_{\parallel}} \right)^{-1}. \quad (3)$$

Here, θ_{\perp} and θ_{\parallel} are the Curie-Weiss temperatures as derived from our dc-susceptibility data (see Fig. 4). Using $\mu_0 H_{\perp \text{res}}^0 = \mu_0 H_{\parallel \text{res}}^0 = 0.25$ T results in a reasonable description of the observed temperature dependence of the resonance field [solid lines in Fig. 7(b)].

Hence, the weak temperature dependence of H_{res} confirms the θ_{\perp} and θ_{\parallel} values, which we extracted from our dc-susceptibility data (Fig. 4). We are also able to explain our magnetization data at about 5 K by a modified g -factor of $g_{\parallel} = 2.2(0)$ under the assumption that internal fields are weak enough. The calculated values are $\mu_{\text{eff}} = 8.7 \mu_{\text{B}}$ and $M_{\text{sat}} = 7.7 \mu_{\text{B}}$ based on this g -factor using the equations mentioned in Sec. III A. These results are close to the values measured by magnetization. The ESR measurements thus confirm the anisotropy of NaGdS_2 .

D. ^{23}Na nuclear magnetic resonance

Figure 8 shows of field-sweep powder NMR spectra at selected temperatures. The powder spectra are described using

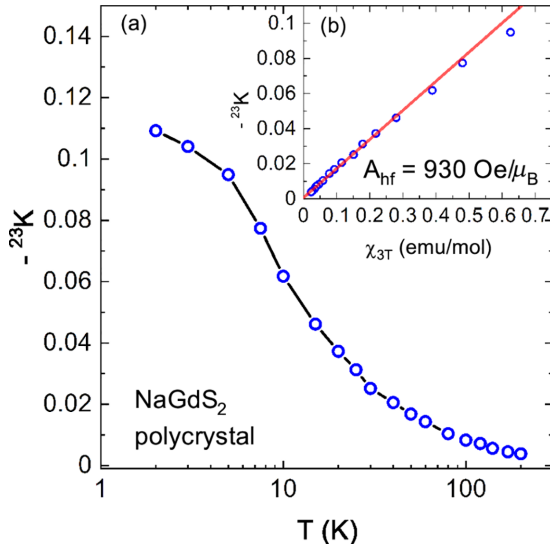


FIG. 9. (a) Temperature dependence of the negative isotropic ^{23}Na lineshift ^{23}K in NaGdS_2 estimated from the 35 MHz field-sweep NMR data (Fig. 8). (b) Knight shift vs. susceptibility (^{23}K - χ plot). Note that here the susceptibility at 3 T was used. The red line shows a fit using Eq. (4) with temperature as implicit parameter.

an anisotropic shift tensor to determine the components for the a , b , and c directions. We determined the isotropic part of the Knight shift, ^{23}K by $^{23}K_{\text{iso}} = (K_a + K_b + K_c)/3$.

While we observed no large anisotropy at high temperatures, the lines below about 10 K, described by two NMR lines, become very broad. One NMR line (labeled 1 in the following) shows an anisotropic broadening below 25 K. Additionally a second NMR signal 2 emerges. The main NMR line 1 has a negative hyperfine field and a negative shift. The line 2 has a positive (ferromagnetic) component. We mentioned the evolution of magnetic fluctuations above in connection with the ESR results (Fig. 6). Overall, an explicit description of the NMR spectrum below 10 K is not possible. Therefore, we only used data above 10 K to analyze the hyperfine coupling. The “Clogston-Jaccarino” plot (^{23}K - χ plot, Fig. 9) relates the NMR shift to the bulk susceptibility. The observed isotropic shift is related to the magnetic bulk susceptibility by

$$^{23}K_{\text{iso}}(T) = K_0 + A_{\text{hf}}\chi(T)/N_A\mu_B, \quad (4)$$

where A_{hf} is the hyperfine coupling constant, χ is the bulk magnetic susceptibility (at the NMR field), and K_0 is a residual temperature-independent contribution. Using this equation, we obtain the hyperfine coupling constant $A_{\text{hf}} = 930 \text{ Oe}/\mu_B$ and a negligibly small K_0 . The value of the hyperfine coupling constant in NaGdS_2 is roughly twice as large as in the NaYbX_2 compounds (above 100 K, where the $S = 7/2$ state dominates the magnetization). The NMR data on the polycrystal can be summarized as follows: The local NMR susceptibility (NMR shift) follows the bulk susceptibility down to approximately 10 K. At lower temperatures, a magnetic anisotropy develops and a new NMR line appears. We interpret this as an indication for the evolution of short-range order in the system, possibly with ferromagnetic origin, typically associated to

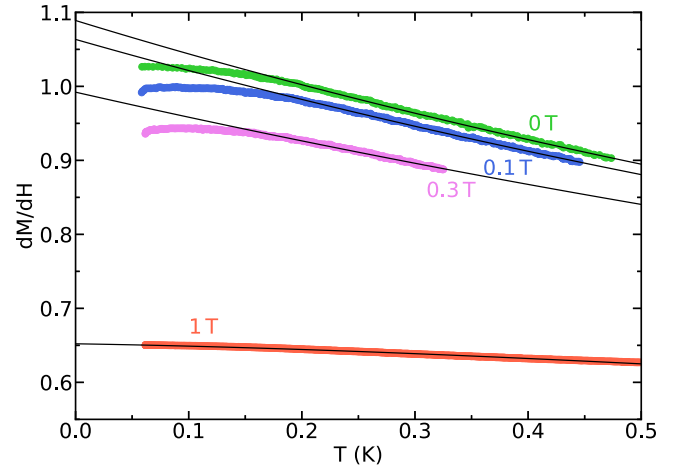


FIG. 10. Temperature-dependent AC susceptibility measured using a μT ac excitation and a frequency of 1123 Hz in zero and various static magnetic fields. The black lines indicate ideal paramagnetic behavior.

dipolar interactions. Results taken at lower fields (9.5 MHz, not shown) are consistent with the 35 MHz data.

E. AC susceptibility at mK temperatures

The ESR and NMR measurements above 2 K evidenced short-range magnetic correlations towards low temperatures, so magnetic order might appear at sub-kelvin temperatures. For this reason, we performed ac-susceptibility measurements at these temperatures in the orientation $H \parallel c$, perpendicular to the Gd^{3+} -layers. First, we performed measurements at various frequencies in zero static magnetic field (123 Hz, 525 Hz, and 1123 Hz). A difference in the result could not be found, so we continued with experiments at the optimized frequency of 1123 Hz (see Fig. 10). We compared the result with the differential susceptibility $\chi_{\text{dif}} = \frac{dM}{dH}$, which was calculated from paramagnetic Brillouin functions, since the Curie law does not apply completely at mK temperatures. We observe a deviation from the paramagnetic Curie law at about 180 mK in zero field. Below this temperature, the susceptibility stays constant and is lower than the paramagnetic susceptibility, indicating dominant antiferromagnetic contributions. However, a sharp cusp is absent, so that a distinct transition representing magnetic order cannot be verified.

To track the deviation from paramagnetism, we performed measurements at different magnetic fields. The deviation from the fully paramagnetic curve remains at about 180 mK for 0.1 T and barely shifts down to about 160 mK for 0.3 T. This shift is again characteristic for an antiferromagnetically dominated behavior. At 1 T the material is finally saturated, as suggested by the magnetization at 0.5 K (see Fig. 3).

F. Thermal expansion and magnetostriction

To further investigate possible magnetic aspects, we performed thermal expansion and magnetostriction measurements at very low temperatures. Due to the plate-like shape of the single crystals, we could only measure length changes

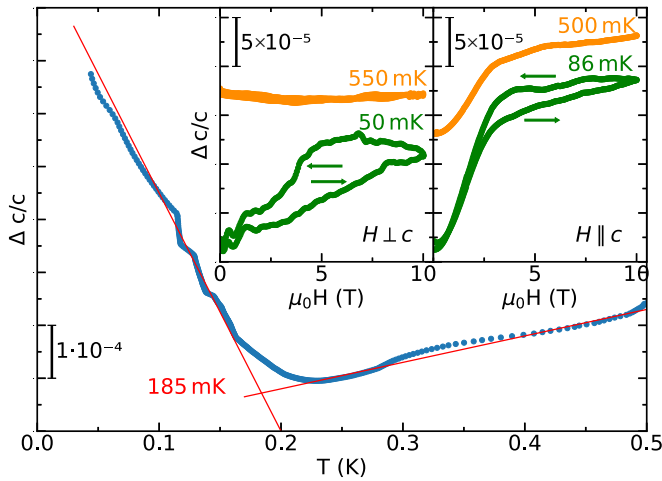


FIG. 11. Thermal expansion along the crystallographic c direction in zero field. The insets show the magnetostriction above and below the slope change occurring at 185 mK for both orientations.

along the c direction ($\Delta c/c$). We applied magnetic fields parallel (longitudinal geometry) and perpendicular (transversal geometry) to c . We measured the relative length change at zero field during cool down and found reproducibly a broad change of slope at about 185 mK, close to the temperature at which the deviation from paramagnetic susceptibility occurs (Fig. 11). The slope $\frac{d}{dT}(\Delta c/c)$ changes from a negative at low temperatures to a smaller positive increase above about 185 mK. We assume that exchange striction is the dominant mechanism [33]. As a result, the distances between the magnetic sites decrease towards lower temperatures. It follows that the ab plane shrinks. Due to the assumed conservation of volume, the c direction should expand towards lower temperatures, which is what we observe below 185 mK. Above this temperature, we see the thermal expansion due to the anharmonic lattice vibration and no magnetic contribution, which indicates paramagnetism. We further measured the magnetostriction for the two field orientations (Fig. 11 insets). For temperatures below the slope change, we found hysteretic behavior, which may be caused by ferromagnetic contributions. Comparing both orientations, the hysteresis loop of the in-plane direction has a larger opening than the loop for out-of-plane field. This indicates a stronger in-plane ferromagnetic contribution than out of plane, which is consistent with magnetization and ESR results. In the paramagnetic phase, apart from the absence of hysteresis, the transversal magnetostriction curve ($H \perp c$) is almost independent of external magnetic field, whereas the longitudinal one ($H \parallel c$) is similar to the magnetization with a saturation at about 3–4 T. The effect of parastriction [34,35] can cause this behavior.

IV. DISCUSSION

The Gd^{3+} -based magnet NaGdS_2 shows paramagnetic behavior with only weak anisotropy at higher temperatures, due to suppressed crystal-field effects [Fig. 4(b)]. However, the Brillouin functions at 2 and 10 K (black lines in Fig. 3) show deviations from the measured magnetization at small

fields. These differences illustrate incipient correlation effects. At low temperatures we indeed found magnetic correlations in ESR, NMR, and magnetization measurements. Susceptibility and dilatometry measurements indicate increasing correlations below about 180 mK as well. Negative Curie-Weiss temperatures indicate predominant antiferromagnetic exchange. However, signs for some ferromagnetic interactions could also be deduced from NMR, magnetization, and magnetostriction measurements, especially for in-plane magnetic fields.

Ferromagnetism caused by dipolar interactions is large enough to induce such an anisotropic effect. A consideration of nearest neighbors supports this assumption. Nearest in-plane Gd^{3+} neighbors have a distance of 4.02 Å, whereas the distance to the nearest out-of-plane neighbor is 7.00 Å.

Low Curie-Weiss temperatures, fast saturation of magnetization data, and strong magnetic-field dependence of the specific heat suggest the presence of only weak exchange interactions. This leads to similar strengths of exchange and dipolar interactions, which may cause additional frustration.

A more detailed description of the energetic conditions in NaGdS_2 is beyond the scope of this work. A similar analysis as done for $\text{KBaGd}(\text{BO}_3)_2$ [22] seems reasonable. We used the *McPhase* program package [36], which provides a Monte Carlo analysis of magnetic interactions using a molecular-field approach. The magnetic Hamiltonian can be written as

$$\mathcal{H} = \mathcal{H}_{\text{ex}} + \mathcal{H}_{\text{dip}}, \quad (5)$$

with Heisenberg exchange (\mathcal{H}_{ex}) and dipole term (\mathcal{H}_{dip}). With the coupling strengths J_{H} and J_{D} , we may write

$$\mathcal{H}_{\text{ex}} = J_{\text{H}} \sum_{\langle ij \rangle} \mathbf{S}_i \cdot \mathbf{S}_j, \quad (6)$$

$$\mathcal{H}_{\text{dip}} = -J_{\text{D}} \sum_{\langle ij \rangle \in d} [\mathbf{S}_i \cdot \mathbf{S}_j - 3(\mathbf{S}_i \cdot \mathbf{e}_{ij})(\mathbf{S}_j \cdot \mathbf{e}_{ij})/r_{ij}^3]. \quad (7)$$

In these expressions, the summation runs over all spins $\mathbf{S}_i, \mathbf{S}_j$, while \mathbf{e}_{ij} and r_{ij} denote the direction and distance between the Gd^{3+} ions i or j , respectively.

We first determined the magnetic structure taking into account only dipolar interactions with

$$J_{\text{D}} = \frac{\mu_0}{4\pi} (g\mu_{\text{B}})^2 \quad (8)$$

using Eq. (7) and summing up all long-range dipole-dipole-interactions up to $d = 23$ Å. Equation (8) uses μ_0 as the permeability of the vacuum, μ_{B} the Bohr magneton, and g the Landé factor. The simulation converges to a ferromagnetic structure of the Gd^{3+} moments in the basal plane, as expected from dipolar interaction, and an antiferromagnetic stacking in the c direction with 120° rotation between neighboring planes. The susceptibility for magnetic fields $H \parallel c$ and $H \perp c$ (field in a direction) results in Curie-Weiss temperatures of $\theta_{\parallel}^{\text{dip}} = -1.1$ K and $\theta_{\perp}^{\text{dip}} = 0.5$ K, respectively. These values are larger than those determined experimentally ($\theta_{\parallel}^{\text{exp}} = -2.2$ K and $\theta_{\perp}^{\text{exp}} = -1.5$ K). This difference, presumably, is due to the exchange interactions.

In regard of the temperature differences $\Delta\theta_k$ ($\Delta\theta_k = \theta_k^{\text{cal}} - \theta_k^{\text{exp}}$, $k = \perp$ or \parallel), J_H could be calculated by

$$J_H = -\frac{3k_B\Delta\theta}{zS(S+1)}, \quad (9)$$

where $z = 6$ is the number of nearest neighbors in the basal plane and $S = 7/2$. Already $J_H = 52$ mK is sufficient to explain the experimental Curie-Weiss temperatures, which is a remarkably low value. Using Eq. (5), we obtain $\theta_{\parallel}^{\text{dip}} = -2.6$ K and $\theta_{\perp}^{\text{dip}} = -1.0$ K.

These results are in good correspondence to our dc-susceptibility measurements. In the experimental case, the anisotropy due to dipolar contributions is reduced by additional quantum-fluctuations, which are not included in this simple model, and slight misalignments in the sample preparation. We have also described the field dependence of the ESR resonance fields by the simulated Curie-Weiss temperatures. Using Eqs. (2) and (3), we were able to obtain the dashed lines in Fig. 7, also resembling the measurement.

In that sense, the delafossite NaGdS₂ represents one of the rare compounds with competing exchange mechanisms (dipolar and Heisenberg) of almost the same energy scale ($J_H = 52$ mK and $J_D/(4.02 \text{ \AA})^3 = 46$ mK). Furthermore, it is noteworthy that dipolar interactions lead to a clear anisotropy in a Gd³⁺ compound without single-ion anisotropy, as also found in the ESR measurements. Both, theoretical and experimental Curie-Weiss temperatures used in Eqs. (2) and (3) describe the ESR measurements well (see solid and dashed line in Fig. 7).

This magnetic behavior with strong dipolar interactions is not new for Gd-based triangular-lattice magnets [21,22,37]. Even Yb-based triangular-lattice magnets can have appreciable dipolar interactions [23].

About a possible order at lower temperatures, we only can speculate. Based on the calculations above, we would expect a stripe-antiferromagnetic order in plane, despite the isotropy of Gd³⁺, caused by strong dipolar interactions.

V. SUMMARY

NaGdS₂ shows paramagnetic behavior with weak anisotropy at high temperatures. However, at lower temperatures sizable magnetic correlations appear in ESR, NMR, and specific-heat data. In particular, we could find signs of antiferromagnetic Heisenberg-type and ferromagnetic dipolar contributions. Moreover, the results indicate that the dipolar interaction leads to an anisotropy at low temperatures. This is seen in stronger ferromagnetic effects for in-plane than out-of-plane magnetic fields.

Susceptibility and dilatometry measurements at very low temperatures show increasing magnetic fluctuations below about 180 mK. This is in accordance to only weak exchange, which corresponds to significantly lower Curie-Weiss temperatures compared to related delafossites. Also magnetization, magnetostriction, and specific-heat data support this fact. Calculations reveal that dipolar and exchange energies are of the same order of magnitude. This leads to the absence of magnetic order down to very low temperatures.

This combination of absent order, weak exchange interactions, and strong dipolar interactions is new for rare-earth delafossites and hints to spin-liquid character also for NaGdS₂.

ACKNOWLEDGMENTS

We acknowledge support from Deutsche Forschungsgemeinschaft (DFG) through SFB 1143 (Project-ID 247310070) and the Würzburg-Dresden Cluster of Excellence on Complexity and Topology in Quantum Matter–*ct.qmat* (EXC 2147, Project No. 390858490). We as well acknowledge the support of the HLD at HZDR, member of European Magnetic Field Laboratory (EMFL).

DATA AVAILABILITY

The data that support the findings of this article are openly available Ref. [38].

-
- [1] M. A. Marquardt, N. A. Ashmore, and D. P. Cann, Crystal chemistry and electrical properties of the delafossite structure, *Thin Solid Films* **496**, 146 (2006).
 - [2] N. Miyasaka, Y. Doi, and Y. Hinatsu, Synthesis and magnetic properties of ALnOGd₂ (A=Cu or Ag; Ln=rare earths) with the delafossite structure, *J. Solid State Chem.* **182**, 2104 (2009).
 - [3] B. Schmidt, J. Sichelschmidt, K. M. Ranjith, T. Doert, and M. Baenitz, Yb delafossites: Unique exchange frustration of 4f spin- $\frac{1}{2}$ moments on a perfect triangular lattice, *Phys. Rev. B* **103**, 214445 (2021).
 - [4] K. M. Ranjith, D. Dmytriieva, S. Khim, J. Sichelschmidt, S. Luther, D. Ehlers, H. Yasuoka, J. Wosnitzer, A. A. Tsirlin, H. Kühne, and M. Baenitz, Field-induced instability of the quantum spin liquid ground state in the $J_{\text{eff}} = \frac{1}{2}$ triangular-lattice compound NaYbO₂, *Phys. Rev. B* **99**, 180401(R) (2019).
 - [5] M. Baenitz, P. Schlender, J. Sichelschmidt, Y. A. Onyukienko, Z. Zangeneh, K. M. Ranjith, R. Sarkar, L. Hozoi, H. C. Walker, J.-C. Orain, H. Yasuoka, J. van den Brink, H. H. Klauss, D. S. Inosov, and T. Doert, NaYbS₂: A planar spin- $\frac{1}{2}$ triangular-lattice magnet and putative spin liquid, *Phys. Rev. B* **98**, 220409(R) (2018).
 - [6] R. Sarkar, P. Schlender, V. Grinenko, E. Haeussler, P. J. Baker, T. Doert, and H.-H. Klauss, Quantum spin liquid ground state in the disorder free triangular lattice NaYbS₂, *Phys. Rev. B* **100**, 241116(R) (2019).
 - [7] K. M. Ranjith, S. Luther, T. Reimann, B. Schmidt, P. Schlender, J. Sichelschmidt, H. Yasuoka, A. M. Strydom, Y. Skourski, J. Wosnitzer, H. Kühne, T. Doert, and M. Baenitz, Anisotropic field-induced ordering in the triangular-lattice quantum spin liquid NaYbSe₂, *Phys. Rev. B* **100**, 224417 (2019).
 - [8] P.-L. Dai, G. Zhang, Y. Xie, C. Duan, Y. Gao, Z. Zhu, E. Feng, Z. Tao, C.-L. Huang, H. Cao, A. Podlesnyak, G. E. Granroth, M. S. Everett, J. C. Neuefeind, D. Voneshen, S. Wang, G. Tan, E. Morosan, X. Wang, H.-Q. Lin *et al.*, Spinon Fermi surface spin liquid in a triangular lattice antiferromagnet NaYbSe₂, *Phys. Rev. X* **11**, 021044 (2021).
 - [9] R. Iizuka, S. Michimura, R. Numakura, Y. Uwatoko, and M. Kosaka, Single crystal growth and physical properties of ytter-

- bium sulfide KYbS₂ with triangular lattice, *JPS Conf. Proc.* **30**, 011097 (2020).
- [10] J. Xing, L. D. Sanjeeva, J. Kim, G. R. Stewart, M.-H. Du, F. A. Reboredo, R. Custelcean, and A. S. Sefat, Crystal synthesis and frustrated magnetism in triangular lattice CsRESe₂ (RE = La–Lu): Quantum spin liquid candidates CsCeSe₂ and CsYbSe₂, *ACS Mater. Lett.* **2**, 71 (2020).
- [11] M. Boswell, Q. Zhang, X. Ke, M. Li, and W. Xie, Triangular lattice of Ho³⁺ with $S_{\text{eff}} = 1/2$ in antiferromagnetic KHoSe₂, *ACS Appl. Electron. Mater.* **6**, 3827 (2024).
- [12] G. Bastien, B. Rubrecht, E. Haeussler, P. Schlender, Z. Zangeneh, S. Avdoshenko, R. Sarkar, A. Alfonso, S. Luther, Y. A. Onyikienko, H. C. Walker, H. Kühne, V. Grinenko, Z. Guguchia, V. Kataev, H. H. Klauss, L. Hozoi, J. van den Brink, D. S. Inosov, B. Büchner *et al.*, Long-range magnetic order in the $\tilde{S} = 1/2$ triangular lattice antiferromagnet KCeS₂, *SciPost Phys.* **9**, 041 (2020).
- [13] A. A. Kulbakov, S. M. Avdoshenko, I. Puente-Orench, M. Deeb, M. Doerr, P. Schlender, T. Doert, and D. S. Inosov, Stripe-yz magnetic order in the triangular-lattice antiferromagnet KCeS₂, *J. Phys.: Condens. Matter* **33**, 425802 (2021).
- [14] M. M. Bordelon, X. Wang, D. M. Pajerowski, A. Banerjee, M. Sherwin, C. M. Brown, M. S. Eldeeb, T. Petersen, L. Hozoi, U. K. Rößler, M. Mourigal, and S. D. Wilson, Magnetic properties and signatures of moment ordering in the triangular lattice antiferromagnet KCoO₂, *Phys. Rev. B* **104**, 094421 (2021).
- [15] S. Zheng, H. Wo, Y. Gu, R. L. Luo, Y. Gu, Y. Zhu, P. Steffens, M. Boehm, Q. Wang, G. Chen, and J. Zhao, Exchange-renormalized crystal field excitations in the quantum Ising magnet KTmSe₂, *Phys. Rev. B* **108**, 054435 (2023).
- [16] C. Delacotte, T. A. Pomelova, T. Stephant, T. Guizouarn, S. Cordier, N. G. Naumov, and P. Lemoine, NaGdS₂: A promising sulfide for cryogenic magnetic cooling, *Chem. Mater.* **34**, 1829 (2022).
- [17] J. A. M. Paddison, H. Jacobsen, O. A. Petrenko, M. T. Fernández-Díaz, P. P. Deen, and A. L. Goodwin, Hidden order in spin-liquid Gd₃Ga₅O₁₂, *Science* **350**, 179 (2015).
- [18] O. A. Petrenko, C. Ritter, M. Yethiraj, and D. M. Paul, Investigation of the low-temperature spin-liquid behavior of the frustrated magnet gadolinium gallium garnet, *Phys. Rev. Lett.* **80**, 4570 (1998).
- [19] A. Keleş and E. Zhao, Absence of long-range order in a triangular spin system with dipolar interactions, *Phys. Rev. Lett.* **120**, 187202 (2018).
- [20] N. Y. Yao, M. Zaletel, D. M. Stamper-Kurn, and A. Vishwanath, A quantum dipolar spin liquid, *Nat. Phys.* **14**, 405 (2018).
- [21] A. Jesche, N. Winterhalter-Stocker, F. Hirschberger, A. Bellon, S. Bachus, Y. Tokiwa, A. A. Tsirlin, and P. Gegenwart, Adiabatic demagnetization cooling well below the magnetic ordering temperature in the triangular antiferromagnet KBaGd(BO₃)₂, *Phys. Rev. B* **107**, 104402 (2023).
- [22] J. Xiang, C. Su, N. Xi, Z. Fu, Z. Chen, H. Jin, Z. Chen, Z.-J. Mo, Y. Qi, J. Shen, L. Zhang, W. Jin, W. Li, P. Sun, and G. Su, Dipolar spin liquid ending with quantum critical point in a Gd-based triangular magnet, *arXiv:2301.03571*.
- [23] R. Bag, M. Ennis, C. Liu, S. E. Dissanayake, Z. Shi, J. Liu, L. Balents, and S. Haravifard, Realization of quantum dipoles in triangular lattice crystal Ba₃Yb(BO₃)₃, *Phys. Rev. B* **104**, L220403 (2021).
- [24] H. Masuda, T. Fujino, N. Sato, and K. Yamada, Electrical properties of Na₂US₃, NaGdS₂ and NaLaS₂, *Mater. Res. Bull.* **34**, 1291 (1999).
- [25] K. Momma and F. Izumi, VESTA3 for three-dimensional visualization of crystal, volumetric and morphology data, *J. Appl. Cryst.* **44**, 1272 (2011).
- [26] M. Rotter, H. Müller, E. Gratz, M. Doerr, and M. Loewenhaupt, A miniature capacitance dilatometer for thermal expansion and magnetostriction, *Rev. Sci. Instrum.* **69**, 2742 (1998).
- [27] D. Ehlers and T. Kurz, Spektrolyst, <http://myweb.rz.uni-augsburg.de/~ehlersdi/spektrolyst/>.
- [28] D. Rauch, M. Kraken, F. J. Litterst, S. Süllow, H. Luetkens, M. Brando, T. Förster, J. Sichelschmidt, A. Neubauer, C. Pfleiderer, W. J. Duncan, and F. M. Grosche, Spectroscopic study of metallic magnetism in single-crystalline Nb_{1-y}Fe_{2+y}, *Phys. Rev. B* **91**, 174404 (2015).
- [29] C. M. Plug, *Crystal Chemistry and Magnetic Properties of Ternary Rare Earth Sulphides* (Rijksuniversiteit Leiden, Dresden, 1977), Chap. IV.5.7, p. 95, https://inis.iaea.org/collection/NCLCollectionStore/_Public/09/364/9364986.pdf.
- [30] M. Duczmal, E. Mosiniewicz-Szablewska, and S. Pokrzywnicki, Electron paramagnetic resonance of Gd³⁺ in TiGdSe₂, *Phys. Stat. Sol. (a)* **196**, 321 (2003).
- [31] J. Sichelschmidt, P. Schlender, B. Schmidt, M. Baenitz, and T. Doert, Electron spin resonance on the spin-1/2 triangular magnet NaYbS₂, *J. Phys.: Condens. Matter* **31**, 205601 (2019).
- [32] D. L. Huber, The effects of anisotropy and Yb-Yb interactions on the low-field electron spin resonance in Yb₂Rh₂Si₂ and YbIr₂Si₂, *J. Phys.: Condens. Matter* **21**, 322203 (2009).
- [33] M. Doerr, M. Rotter, and A. Lindbaum, Magnetostriction in rare-earth based antiferromagnets, *Adv. Phys.* **54**, 1 (2005).
- [34] B. Bernáth, K. Kutko, S. Wiedmann, O. Young, H. Engelkamp, P. C. M. Christianen, S. Poperezhai, L. V. Pourousski, S. Khmelevskiy, and D. Kamenskiy, Massive magnetostriction of the paramagnetic insulator KEr(MoO₄)₂ via a single-ion effect, *Adv. Electron. Mater.* **8**, 2100770 (2022).
- [35] A. Bienkowski and R. Szewczyk, Magnetostrictive properties of Mn_{0.70}Zn_{0.24}Fe_{2.0604} ferrite, *Materials* **11**, 1894 (2018).
- [36] M. Rotter, McPhase Manual (2024), <https://mcphase.github.io/webpage/manual/manual.html>.
- [37] S. Guo, T. Kong, W. Xie, L. Nguyen, K. Stolze, F. A. Cevallos, and R. J. Cava, Triangular rare-earth lattice materials RbBaR(BO₃)₂ (R = Y, Gd-Yb) and comparison to the KBaR(BO₃)₂ analogs, *Inorg. Chem.* **58**, 3308 (2019).
- [38] J. Grumbach, E. Häußler, S. Luther, J. Sichelschmidt, K. M. Ranjith, T. Herrmannsdörfer, M. Rotter, S. Granovsky, H. Kühne, M. Uhlarz, J. Wosnitzer, H.-H. Klauß, M. Baenitz, T. Doert, and M. Doerr, Data underpinning: Magnetic anisotropy and dipolar interactions in the frustrated triangular-lattice magnet NaGdS₂ (2025), <https://datashare.tu-dresden.de/s/fxemEEPr9pnW23J>.